PCCP

Cite this: *Phys. Chem. Chem. Phys.*, 2011, **13**, 19848–19855

www.rsc.org/pccp

PAPER

Probing the interaction of amorphous solid water on a hydrophobic surface: dewetting and crystallization kinetics of ASW on carbon tetrachloride

R. Alan May, R. Scott Smith* and Bruce D. Kay*

Received 8th June 2011, Accepted 31st July 2011
DOI: 10.1039/c1cp21855g

Desorption of carbon tetrachloride from beneath an amorphous solid water (ASW) overlayer is explored utilizing a combination of temperature programmed desorption and infrared spectroscopy. Otherwise inaccessible information about the dewetting and crystallization of ASW is revealed by monitoring desorption of the CCl_4 underlayer. The desorption maximum of CCl_4 on graphene occurs at ~140 K. When ASW wets the CCl_4 no desorption below 140 K is observed. However, the mobility of the water molecules increases with ASW deposition temperature, leading to a thermodynamically driven dewetting of water from the hydrophobic CCl_4 surface. This dewetting exposes some CCl_4 to the ambient environment, allowing unhindered desorption of CCl_4 below 140 K. When ASW completely covers the underlayer, desorption of CCl_4 is delayed until crystallization induced cracking of the ASW overlayer opens an escape path to the surface. The subsequent rapid episodic release of CCl_4 is termed a "molecular volcano". Reflection absorption infrared spectroscopy (RAIRS) measurements indicate that the onset and duration of the molecular volcano is directly controlled by the ASW crystallization kinetics.

1. Introduction

Water is fundamental to a staggering array of processes ranging across disciplines such as biology,[1,2] chemistry,[3] and astrophysics.[4] Interest in water stems from its ubiquity and numerous, often anomalous, properties such as the apparent oxymoron of hydrophobic ice.[5] Another remarkable phase of water, known as amorphous solid water (ASW) forms when water is deposited upon a substrate cooled below 130 K. ASW is kinetically metastable and transforms to a thermodynamically stable crystalline phase upon heating.[6] Because it is thermodynamically continuous with supercooled liquid water,[7,8] interest in ASW is driven by its promise as a model for liquid water. Additionally, ASW is an excellent platform for studying the crystallization kinetics of metastable materials[8,9] and the unique properties of porous films deposited *via* ballistic deposition.[10–18]

The development of advanced characterization techniques has greatly enhanced understanding of the conditions giving rise to water's kaleidoscope of properties. However, fully understanding the behavior of water requires further experimental refinement. For example, the adsorption of inert gases, such as Ar or Kr, has been utilized to determine the structure of water on various substrates because desorption from water occurs at a distinct temperature compared to desorption from substrates such as Pt(111), Pd(111), and graphene.[5,19–21] Unfortunately, the rare gas desorption technique cannot be utilized to study systems where this contrast in desorption temperature is negligibly small. For example, Kr desorbs at approximately the same temperature from multilayers of ASW or CCl_4. Therefore, alternative methods must be developed to explore the ASW/CCl_4 system. Here we describe a new way to characterize the process of dewetting and crystallization of ASW by monitoring two distinct pathways of CCl_4 desorption from beneath ASW.

The interaction of water with a hydrophobic surface is important for understanding many industrial and biological processes.[22,23] The canonical wisdom is that water on a hydrophobic surface clusters to form structures that maximize the number of hydrogen bonds, thus lowering the overall energy of the system. While exact determination of the energetics of ASW interaction with CCl_4 is difficult, the formation of water clusters is expected because bulk water has a surface energy approximately three times that of CCl_4.[24,25] Recent theoretical and experimental investigations have focused on the molecular level structure at the liquid water/hydrophobic substrate interface.[22,26–31] Despite this, more work is needed to further our understanding of water on hydrophobic surfaces.

Fundamental and Computational Sciences Directorate, Pacific Northwest National Laboratory, Richland, Washington 99352. E-mail: Scott.Smith@pnnl.gov, Bruce.Kay@pnnl.gov

The present study focuses on the interactions of vapor deposited water on a hydrophobic CCl_4 substrate. Temperature programmed desorption (TPD) and reflection absorption infrared spectroscopy (RAIRS) are used to probe the structure and crystallization kinetics of water deposited on CCl_4 layers. Water deposited at low temperatures appears to "wet" the hydrophobic surface whereas at higher temperatures the deposited water clearly dewets from CCl_4. The overall picture is that at low temperature, the adsorbed water does not have enough thermal energy to surmount the kinetic barriers to form the lower energy water clusters, and thus "kinetically" wets the surface.[5,19–21] As the deposition temperature is increased more of the deposited water can dewet from the surface. Molecules underneath the ASW are restricted from desorbing while exposed CCl_4 molecules are free to desorb unimpeded. As a result, the exposed fraction of CCl_4 can be determined by monitoring CCl_4 desorption and used to determine the extent of dewetting. Dewetting is shown to be a function of both water coverage and temperature. Desorption of covered CCl_4 is dictated by the ASW overlayer and proceeds through a desorption event termed the "molecular volcano".

First described by Smith *et al.*,[32] the "molecular volcano" arises from the sudden episodic release of an immiscible underlayer, CCl_4, due to the formation of cracks through a crystallizing amorphous solid water overlayer. Later, this was shown to be a general phenomenon with N_2, Ar, O_2, CO, and CH_4 exhibiting similar volcanic behavior. The similarity between the desorption of this wide variety of gases is strong indication that the molecular volcano reports primarily on morphological changes occurring during the crystallization of ASW.[4] Hence, the position and intensity of the CCl_4 volcano gives important information about the crystallization of ASW as indicated by simultaneously acquired RAIRS and TPD measurements.

2. Experimental

Experiments were performed in an ultra high vacuum system (UHV), described previously,[16,33] utilizing a 1-cm diameter Pt(111) substrate spot-welded to tantalum leads and cooled with a closed cycle He cryostat. This system has a base pressure of $<1 \times 10^{-10}$ Torr and base temperature of $\sim$25 K which can be controlled up to 1200 K by resistive heating. Temperature was measured by a type K thermocouple spot-welded to the back of the Pt(111) substrate and calibrated to an accuracy of better than $\pm$2 K utilizing the controlled desorption of Kr and H_2O. The Pt(111) substrate was cleaned by Ne^+ ion sputtering at 1.5 kV followed by O_2 exposure and subsequent UHV annealing at 1000 K. After cleaning and annealing, graphene was deposited by heating the Pt(111) substrate to 1100 K in the presence of decane, resulting in a single layer of carbon with graphene structure.[5,34] The integrity of this layer was verified by desorption of Kr and H_2O multilayers.

Carbon tetrachloride (Sigma-Aldrich $\geq$ 99.9%) and water (doubly distilled 18 MΩ-cm) were deposited at normal incidence *via* quasi-effusive molecular beams. The CCl_4 beam was formed by expanding 1 Torr of room temperature CCl_4 gas through a 1-mm diameter orifice. The beam passed through four differential pumping stages before impinging on the sample at a rate of 0.143 ML/s with a diameter of 0.75 cm. A ML of CCl_4 is defined as the monolayer saturation of CCl_4 on graphene while a ML of water is defined as the monolayer saturation of H_2O on Pt(111). The water beam was formed by expanding 2 Torr of water vapor through a 1-mm diameter orifice. The beam was collimated by three stages of differential pumping before impinging on the sample at a rate of 0.87 ML/s with a beam diameter slightly larger than the 1-cm diameter of the Pt(111) substrate.

TPD spectra were obtained at a ramp rate of 0.6 K/s with desorption detected utilizing an Extrel quadrapole mass spectrometer in a line of sight configuration. CCl_4 was monitored using the fragment $m/z = 47$ while water was monitored at $m/z = 18$. The intensity of the mass spectrometer signal was converted into an absolute desorption rate by utilizing the area under the monolayer desorption peak of CCl_4 on graphene and H_2O on Pt(111). RAIRS spectra were recorded with a Bruker Equinox 55 Fourier transform infrared (FTIR) spectrometer at an $82^\circ \pm 1^\circ$ angle of incidence using a liquid nitrogen cooled mercury cadmium telluride (MCT) detector. For concurrent TPD/RAIRS experiments the temperature was ramped at 0.6 K/s. RAIRS spectra, 4 average scans with a 4 cm^{-1} resolution, were taken approximately every 1 K.

3. Results and discussion

3.1 Origins of the molecular volcano

When H_2O is deposited on low temperature substrates, it forms a kinetically metastable amorphous phase known as amorphous solid water (ASW).[6,35] ASW deposited at normal incidence is dense and continuous as confirmed with nitrogen physisorption and infrared spectroscopy.[12,17] The interaction of CCl_4 with ASW has been previously studied by us[32] and others.[36,37] When heated, ASW begins to crystallize. This crystallization induces cracking which opens a connected pathway between the underlayer and the external environment.[4,32] Fig. 1(a) displays a schematic of two experiments which illustrate this phenomenon. In the first experiment, 5 ML of CCl_4 was deposited on a graphene substrate at 25 K (with no ASW overlayer) and subsequently heated at a rate of 0.6 K/s. The CCl_4 desorption spectrum is displayed in Fig. 1(b) (red dashed line). Multilayer desorption begins at $\sim$130 K and peaks at $\sim$140 K when the multilayers of CCl_4 are exhausted. The first monolayer of CCl_4 physisorbs more strongly to the graphene and persists to $\sim$164 K where a small peak is observed. The second experiment exhibits very different behavior. The CCl_4 has been capped with 30 ML of ASW (Fig. 1(b), red solid line) and no desorption is observed at the previous peak of 140 K. Instead, the ASW overlayer prevents CCl_4 desorption until the advent of a sharp desorption peak with a maximum at 158 K. This sudden release of CCl_4 is an example of the "molecular volcano".[4,32] The volcano occurs in concert with a low temperature shoulder in the H_2O TPD spectrum (Fig. 1(b), blue solid line). This shoulder indicates a transition from the kinetically metastable ASW to thermodynamically stable crystalline ice (CI).[7,8] The CI has a lower vapor pressure than ASW resulting in a $\sim$2x decrease in

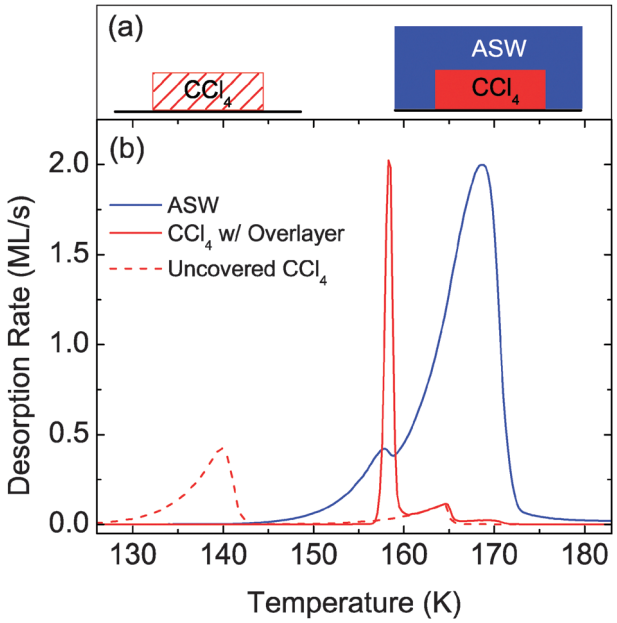

Fig. 1 (a) Schematic of two desorption experiments shown below. (b) Temperature programmed desorption performed at a rate of 0.6 K/s on 5 ML CCl_4 (dashed red line) deposited on graphene and 5 ML CCl_4 (solid red line) with a 30 ML ASW overlayer (solid blue line).

the desorption rate.[7,8] Crystallization induces cracking in the overlayer. Upon reaching a critical threshold these cracks form a connected pathway through the ASW overlayer which allows CCl_4 to rapidly escape. The distinct desorption behavior of exposed (dashed red line) and covered (solid red line) CCl_4 observed in Fig. 1 provides a method to probe the structure of the ASW overlayer. We now present results which indicate the importance of the ASW overlayer thickness and deposition temperature to the CCl_4 desorption spectra.

Fig. 2(a) displays the CCl_4 desorption spectra for various ASW overlayer thicknesses (0 to 50 ML) deposited on 5 ML of CCl_4 at 25 K. The spectra show that the position of the molecular volcano is pushed out to higher temperatures as the ASW overlayer thickness increases. The eruption of the volcano is dependent upon the formation of connected pathways from the exposed surface of the overlayer to the CCl_4 reservoir underneath. The formation of these pathways depends upon the crystallization kinetics of the overlayer. Thus, the volcano desorption peak moves to higher temperatures with increasing layer thickness because connected pathways take longer to form in the thicker ASW. This result is consistent with several studies which indicate that the crystallization kinetics slow down with increasing ASW thickness[9,38–41] until they stabilize at the thick film limit.[42]

Changing the deposition temperature of ASW has also been shown to alter the crystallization kinetics. Higher deposition temperatures seed nucleation sites that increase the crystallization rate.[38,40,42] Therefore, increasing the ASW deposition temperature should shift the molecular volcano to lower temperatures compared to an equivalent overlayer thickness deposited at 25 K. Fig. 2(b) displays CCl_4 desorption spectra for various ASW overlayer thicknesses (0 to 50 ML) deposited on 5 ML of CCl_4 at 110 K. The TPD spectra clearly illustrate

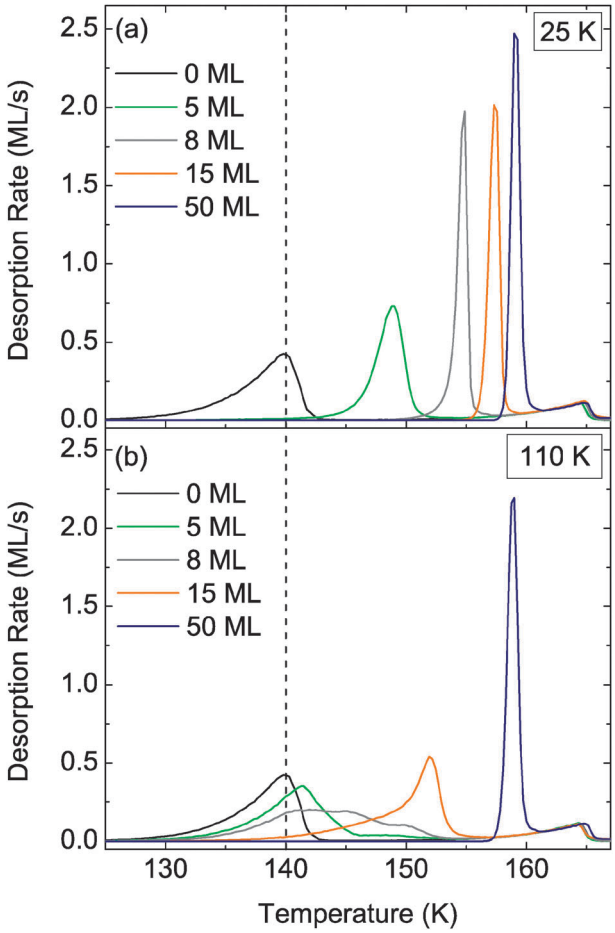

Fig. 2 TPD spectra of 5 ML CCl_4 desorption from a graphene surface as a function of ASW overlayer thickness at an ASW deposition temperature of (a) 25 K and (b) 110 K.

that the ASW deposition temperature does affect the position of the volcano peak, at least for overlayers less than 50 ML equivalents. Volcano desorption from the 15 ML overlayer broadens significantly and decreases from 157 K in Fig. 2(a) to 152 K in Fig. 2(b), while desorption from 8 ML and 5 ML overlayers has lost nearly all volcano character, with significant amounts of desorption occurring below 140 K. Interestingly, the line shape of TPD spectra below 140 K is similar to desorption of uncovered CCl_4, suggesting that desorption below 140 K arises from uncovered CCl_4 and not the volcano. No significant changes in the TPD spectra were observed by annealing the CCl_4 before ASW overlayer deposition or by annealing the entire structure after deposition of the ASW layer (data not shown), implying that the observed changes in the CCl_4 TPD spectra reflect morphological changes in the ASW overlayer occurring during deposition.

Fig. 3 displays the dependence of 5 ML CCl_4 desorption through a 15 ML thick ASW overlayer on the deposition temperature of ASW. The ASW deposition times were adjusted to account for the decreasing condensation coefficient of water at deposition temperatures above 110 K. A similar observation of reduced water condensation with increasing temperature on octane has been reported previously and reflects the weaker interaction of water vapor with the

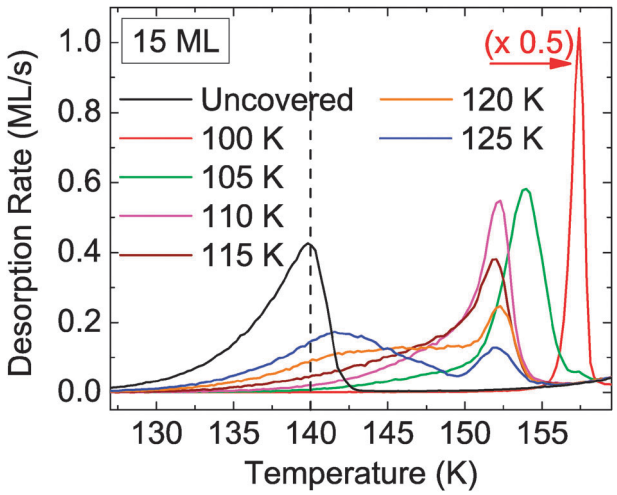

Fig. 3 Desorption spectra of 5 ML of CCl_4 covered with 15 ML of ASW at various ASW deposition temperatures.

hydrophobic substrate.[43] Depositions at substrate temperatures below 100 K are observed to be qualitatively similar to deposition at 100 K, so they have been omitted for clarity. At 100 K, abrupt desorption of CCl_4 results in a volcano peak similar to that shown in Fig. 1(b). Increasing the ASW deposition temperature from 100 K to 105 K broadens the volcano and decreases the desorption peak by 4 K. Again, this temperature shift is attributed to changes in the crystallization kinetics and is strongly correlated to RAIRS spectra discussed below. Increasing the deposition temperature to 110 K shifts the volcano peak lower by another 2 K. Interestingly, the center of the volcano peak for ASW deposition temperatures above 110 K remains relatively constant. This finding is consistent with the work of Dohnálek *et al.*[38] who showed that ASW crystallization kinetics become substrate deposition temperature independent above a certain temperature. Even though the volcano peak position remains constant, the volcano intensity decreases when H_2O is deposited at elevated temperatures (>110 K). The volcano peak intensity decreases with increasing deposition temperature (Fig. 3) because of the emergence of a second desorption pathway below 140 K. Desorption in this low temperature region is similar in shape to that of unhindered CCl_4 and is indicative of ASW dewetting from the "hydrophobic" CCl_4.

Two distinct desorption regions are observed: one occurring at high temperatures commensurate with crystallization of the ASW overlayer (molecular volcano) and a second associated with a lower temperature mechanism which is an attenuated version of unhindered CCl_4 desorption. The appearance of a free (unhindered) CCl_4 desorption pathway at higher deposition temperatures indicates that the H_2O overlayer is not completely wetting the hydrophobic CCl_4 surface. In Fig. 1(b), the molecular volcano is observed because kinetically metastable ASW completely covers the CCl_4 underlayer preventing desorption until crystallization induced cracking opens an escape pathway to the surface. Similarly, TPD spectra of ASW deposited at ≤ 100 K indicate negligible desorption below the onset of the molecular volcano. However, when the ASW deposition temperature is increased, the adsorbing H_2O molecules become more mobile and dewet to minimize their interaction with the hydrophobic CCl_4. This dewetting exposes areas of the CCl_4 directly to vacuum, creating regions where CCl_4 desorbs in the same manner as the uncovered case in Fig. 1(b). The nature of dewetting and the demarcation of these two distinct desorption regions are further elucidated by the integration of RAIRS to simultaneously capture changes in infrared absorbance during TPD.

3.2 Infrared studies of ASW crystallization

The crystallization of ASW can be monitored using RAIRS by observing the growth of an intense peak in the O–H stretch region of H_2O at 3247 cm^{-1}.[8] Fig. 4(a) displays the infrared spectrum for H_2O deposited at 25 K. The broad absorbance centered at 3400 cm^{-1} (black line) is consistent with previously reported infrared measurements of ASW.[8,16,44] Upon heating, a sharp absorbance feature centered at 3247 cm^{-1}, becomes prominent and signals crystallization (red line). Thus, the RAIRS technique makes two important contributions to this work. First, RAIRS helps to determine the onset of crystallization. Second, as will be shown, it further correlates the molecular volcano to the crystallization kinetics of ASW.

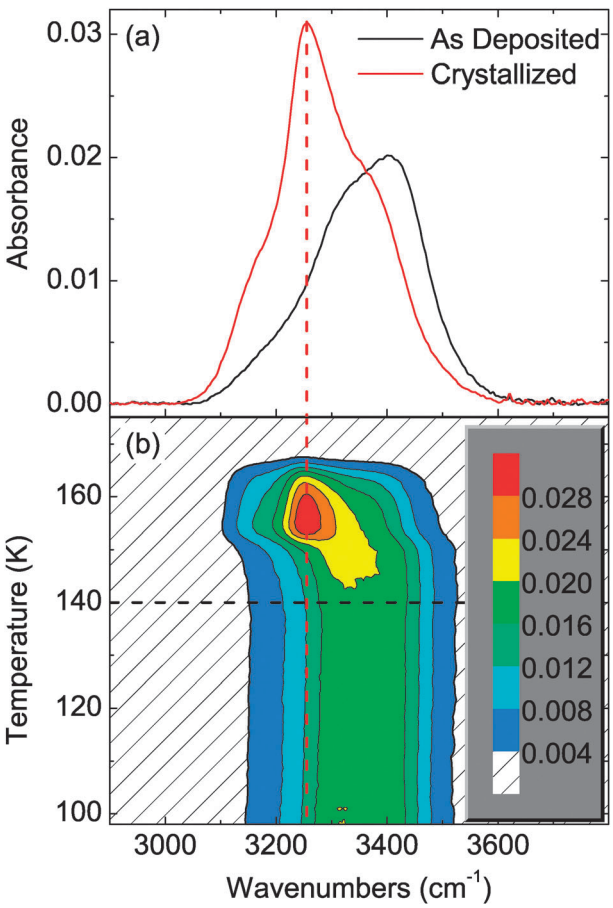

Fig. 4 (a) Infrared spectra of a 15 ML ASW film deposited at 25 K (black line) and after heating (red line) to 160 K. The growth of a peak at 3247 cm^{-1} indicates water crystallization. (b) Contour plot of infrared spectra taken during TPD at 0.6 K/s of a 15 ML water overlayer deposited at 110 K. There is approximately one spectrum per degree.

A time series of RAIRS spectra obtained during TPD at 0.6 K/s for a 15 ML water overlayer deposited on 5 ML CCl_4 at 110 K is shown as a contour plot in Fig. 4(b). Below 140 K the O–H stretching region remains unchanged, qualitatively similar to the "as deposited" spectrum in Fig. 4(a). Above 140 K the peak intensity increases and begins to red shift from a maximum at 3400 cm^{-1} to 3247 cm^{-1}. Upon reaching ~160 K, H_2O desorption dominates leading to a decrease in absorbance until the water completely desorbs. The spectra in Fig. 4(b) clearly show that below 140 K (horizontal dashed line) there is no detectable crystallization of the ASW overlayer. The crystallization kinetics that commence above 140 K can be obtained from a cut at constant frequency through the time series of spectra.[8,35]

Fig. 5(a) displays cuts at 3247 cm^{-1} through time series of RAIRS spectra for various water overlayer thicknesses deposited at 110 K. As was observed in Fig. 4(b), no significant absorbance increase occurs below 140 K (vertical dashed line), even for ASW overlayer thicknesses as small as 5 ML.

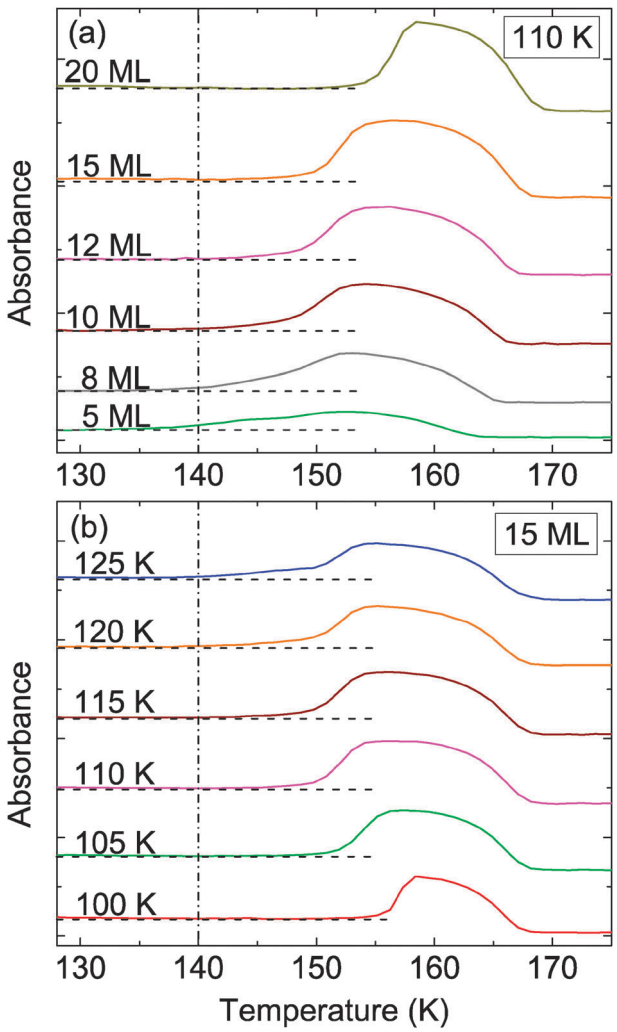

Fig. 5 Cuts through FTIR spectra at 3247 cm^{-1} during TPD at a rate of 0.6 K/s for (a) H_2O overlayers from 5 ML to 20 ML deposited at 110 K and (b) 15 ML ASW overlayer deposited at temperatures ranging from 100 K to 125 K.

Horizontal dashed lines that extend the low temperature baselines are provided to guide the eye. The data show that the onset of crystallization, defined as an absorbance increase above the low temperature baseline, shifts to higher temperature with increasing overlayer thickness. These results are consistent with the desorption experiments in Fig. 2(a) which show the temperature of the volcano peak shifts to higher temperature with increasing overlayer thickness. As stated previously, the slowing of the crystallization kinetics with overlayer thickness has been observed by several investigators[9,38,39,42] even though a comprehensive molecular level understanding remains elusive.

Fig. 5(b) displays the results of similar experiments except that here the ASW overlayer thickness was held constant at 15 ML and the ASW deposition temperature was varied. Again, the data show that the onset of measurable crystallization always occurs above 140 K and shifts to lower temperature with increasing deposition temperature. These results are consistent with the TPD observations in Fig. 2(b) that showed for equivalent overlayer thicknesses, the CCl_4 volcano desorption peak shifts to lower temperature at higher ASW deposition temperatures. The temperature dependence of crystallization is explained by the formation of crystalline nuclei at higher deposition temperatures, so called pre-seeding, which leads to the earlier onset of crystallization.[33,38,42] This effect is observed for a 15 ML ASW overlayer deposited at temperatures up to 125 K in Fig. 5(b). ASW deposited at 100 K crystallizes rather abruptly as indicated by the steep rise in absorbance at ~157 K in Fig. 5(b). Increasing the deposition temperature shifts the onset of crystallization to lower temperatures. At deposition temperatures of 120 K and 125 K a more subtle, slowly increasing absorbance feature (originating at 140 K) is observed before the onset of rapid crystallization. The initial slow increase is likely due to crystallization around preseeded nucleation sites proceeding slowly until new nuclei are formed at higher temperatures. These nuclei rapidly increase the crystallization rate, as indicated by steepening of the curves above ~150 K.

The main results of Fig. 5 are twofold. First, while the crystallization temperature of the ASW overlayer is dependent on thickness and deposition temperature, the onset of crystallization is always above 140 K. Thus, desorption of CCl_4 below 140 K (Fig. 2 and 3) is not mediated by the crystallization of ASW. Second, there is a qualitative correlation between the volcano desorption peak temperatures in Fig. 2 and the onset of crystallization observed in Fig. 5.

The correlation between the CCl_4 volcano desorption peak and ASW crystallization is highlighted in Fig. 6 where CCl_4 TPD volcano peaks (solid lines, arbitrary units) from 15 ML ASW overlayers are plotted along with the corresponding absorbance cuts at 3427 cm^{-1} (dashed lines) through the RAIRS spectra. The results for four different ASW deposition temperatures are shown. For all of the deposition temperatures, the leading edge of the infrared absorbance and TPD spectra exhibit qualitatively similar temperature dependence. As the deposition temperature is increased the initial absorbance increases proportional to the greater degree of crystallinity resulting from the higher substrate deposition temperature. The peak of the molecular volcano (demarked by an open circle) occurs at 0.015 ± 0.001 absorbance units

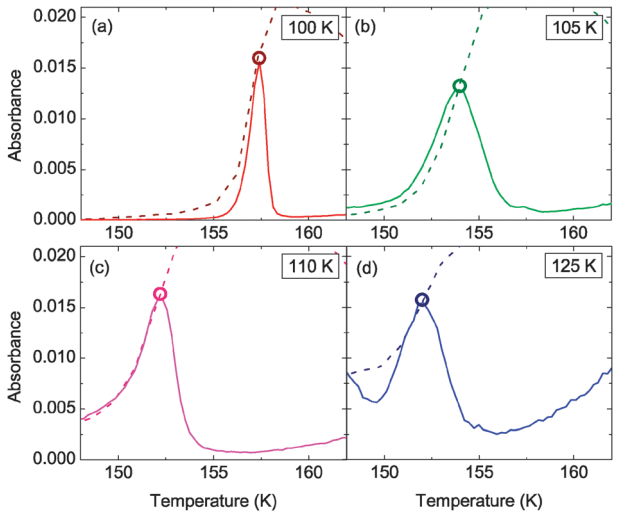

Fig. 6 RAIRS traces at 3247 cm^{-1} (dashed lines) and TPD spectra (solid lines) of 15 ML ASW overlayers crystallizing during TPD at 0.6 K/s. Circles indicate the peak of the molecular volcano, for each temperature the volcano release occurs after the infrared absorbance has increased to 0.015 ± 0.001.

irrespective of deposition temperature. It is clear from Fig. 6 that the eruption of the molecular volcano is highly correlated with the degree of crystallization, occurring reproducibly at the same extent of crystallization regardless of deposition temperature.

In summary, RAIRS indicates that there is a direct correlation between the temperature of the volcano peak and the crystallization kinetics of ASW. CCl_4 desorbing from the volcano is initially covered by ASW and is released by crystallization induced cracking of the overlayer. However, under certain conditions CCl_4 desorbs below 140 K and, as will be shown, this desorption precedes the crystallization of ASW.

3.3 Dewetting of ASW on a hydrophobic CCl_4 substrate

In previous efforts, the extent of dewetting on substrates such as Pt(111), Pd(111), and graphene has been determined by inert gas probes, *i.e.* Kr, which exhibit very different desorption behavior based on the adsorption environment.[5,19–21] However, this method cannot be used for this system because Kr physisorbed to CCl_4 or ASW multilayers has similar desorption characteristics. Fortunately, the relative amount of exposed CCl_4 surface area can be determined by monitoring desorption of the CCl_4 in the region below 140 K. Log plots of TPD spectra for CCl_4 desorption are displayed in Fig. 7 and clearly indicate a distinct pattern of desorption below 140 K. Fig. 7(a) displays the TPD spectra for various thicknesses (0 to 50 ML) of H_2O deposited at a substrate temperature of 110 K. Under these conditions, the low temperature desorption leading edges from ASW overlayer thicknesses up to 20 ML are linear and highly parallel. With increasing ASW overlayer thickness, the CCl_4 desorption rates decrease until a thickness of 50 ML, where there is no low temperature (<140 K) desorption above the baseline. This is consistent with the results in Fig. 1(b) that show that CCl_4 will not desorb as long as it is completely covered by ASW. Therefore, desorption below 140 K is

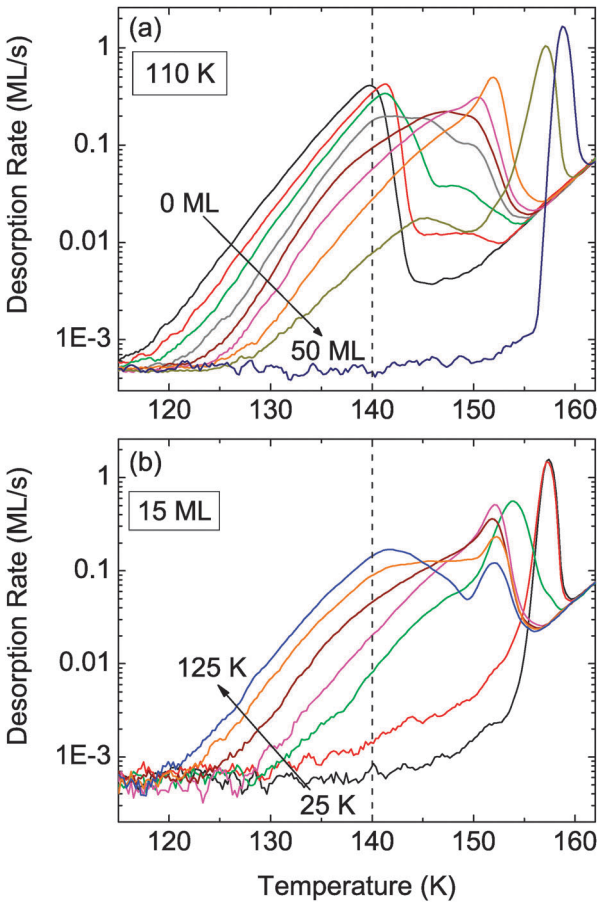

Fig. 7 Log plots of CCl_4 desorption in the dewetting region during TPD at 0.6 K/s for 5 ML CCl_4 on graphene with (a) ASW overlayers of 0, 2, 5, 8, 10, 12, 15, 20, and 50 ML deposited at 110 K and (b) 15 ML ASW overlayer with deposition temperatures of 25, 100, 105, 110, 115, 120, and 125 K.

attributed to uncovered CCl_4. Since there is uncovered CCl_4, H_2O must be dewetting either during deposition or during the TPD ramp prior to desorption. Given that overlayers ≥ 5 ML deposited at 25 K exhibit no dewetting and that post-deposition annealing had negligible effect on resulting TPD spectra (data not shown) it is most likely that the majority of dewetting occurs during deposition (at least for overlayers ≥ 5 ML). This is expected as the adsorbing H_2O molecules are more mobile during deposition than when locked inside the ASW matrix, and is consistent with previous work.[9,38] Thus the amount of CCl_4 which desorbs below 140 K decreases with increasing coverage of H_2O because increasingly larger portions of the surface become covered by ASW. Similarly, at a given thickness, desorption of CCl_4 below 140 K is enhanced by an increase in the ASW deposition temperature. Higher deposition temperatures lead to increased surface mobility of adsorbing H_2O, allowing for the formation of three-dimensional H_2O clusters which exposes more of the hydrophobic CCl_4 substrate.

A possible alternative explanation for this phenomenon is that water displaces CCl_4 during deposition, causing the CCl_4 to float on top of the ASW and potentially leading to many of the discussed observations. However, contributions to the observed dewetting behavior by water displacement of CCl_4

have been ruled out. First, as observed by Sadtchenko *et al.*[37] CCl_4 has a distinct desorption pattern on ASW. Desorption of submonolayer amounts of CCl_4 from ASW occurs ~10 K before the onset of multilayer desorption from graphene while the addition of more CCl_4 leads to the formation of two distinct desorption peaks from ASW. Here, only a single multilayer desorption peak is observed for CCl_4 with a desorption temperature consistent with multilayer desorption from graphene (Fig. 3). Thus, based on the temperature dependence of the CCl_4 desorption we can exclude the displacement of CCl_4 during water deposition as the primary mechanism for the experimental results presented here. Second, the negligible contribution of the displacement of CCl_4 by ASW to the TPD spectra is consistent with other experimental results where methanol is deposited on top of rare gas layers.[45–48] In those experiments only a small fraction of the rare gas (<5% of a monolayer) was observed to be displaced for overlayers a few ML thick. Because of its larger polarizability compared the rare gases (*e.g.* 10.5×10^{-24} cm^3 for CCl_4 and 2.48×10^{-24} cm^3 for Kr) we would expect the amount of displacement for CCl_4 to be even less.

The effects of ASW deposition temperature on dewetting are confirmed in Fig. 7(b), which displays log plots of TPD spectra for CCl_4 desorption from a 15 ML ASW overlayer deposited at temperatures ranging from 25 to 125 K. While desorption below 140 K is negligible when ASW is deposited at 25 K, increasing the deposition temperature to 100 K leads to a discernable increase in the desorption of CCl_4 below 140 K, thus signaling the onset of the dewetting process. Increasing the deposition temperature in 5 K increments from 100 K to 125 K shifts the TPD of CCl_4 to lower temperature, consistent with facilitation of dewetting by the higher deposition temperature.

The fraction of the CCl_4 surface that is not covered with ASW can be obtained by analyzing the leading edge of the desorption spectra below 140 K. The exposed fraction is simply the ratio of the leading edge desorption rate divided by the desorption rate from a film with no ASW overlayer, here determined at 135 K. The ASW covered fraction is simply the one's complement of the exposed fraction. The fraction of CCl_4 covered by ASW depends on both the thickness and deposition temperature of the ASW overlayer. Fig. 8 displays the covered fraction *versus* ASW coverage at various deposition temperatures for more than 100 experiments. At all deposition temperatures the covered fraction increases with ASW coverage albeit with different coverage dependencies. With increasing deposition temperature the amount of water required to completely cover the CCl_4 increases. For example at 25 K, CCl_4 is completely covered by 5 ML, whereas at 125 K this same amount of water is sufficient to cover only ~17% of the surface. In fact, at 125 K the low temperature (<140 K) CCl_4 desorption is not quenched until 50 ML equivalents of water are deposited.

Statistically random deposition yields a covered fraction that scales as $1 - e^{-\theta}$ with increasing ASW overlayer coverage, θ, as shown by the dashed line in Fig. 8.[20] The 25 K experimental data cover the CCl_4 underlayer more slowly than random deposition and exhibit an ASW coverage dependence roughly described by $1 - e^{-0.3\cdot\theta}$ suggesting that some

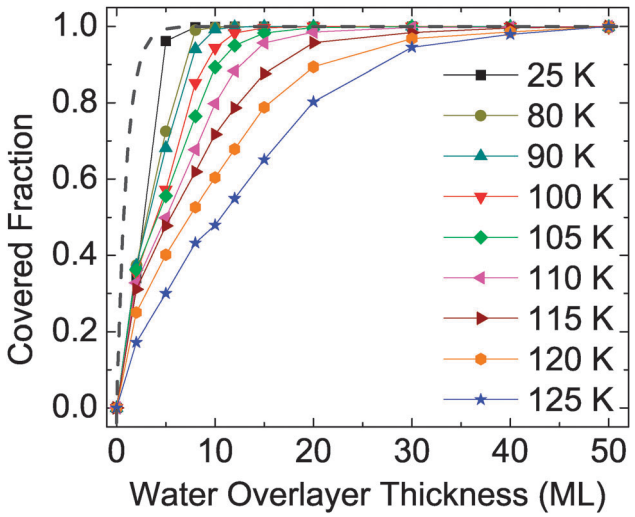

Fig. 8 Relative amount of CCl_4 covered by ASW as a function of water overlayer thickness and deposition temperature as derived from desorption of CCl_4 at 135 K during TPD at a ramp of 0.6 K/s. The dashed black line corresponds to random deposition of the ASW overlayer.

dewetting occurs even at 25 K. However, for very thin ASW overlayers significant rearrangement during the TPD heating ramp cannot be ruled out since our experiments are insensitive to any dewetting that occurs prior to the onset of measurable CCl_4 desorption at ~120 K.

Fig. 8 reveals that the interaction of ASW with the hydrophobic CCl_4 surface depends on both the amount of ASW deposited and the deposition temperature. At low deposition temperatures ASW can kinetically "wet" the hydrophobic CCl_4 layer. However, as the deposition temperature is increased adsorbing water molecules become more mobile and are able to adopt a lower-energy dewetted structure. The lower energy configuration involves the formation of an increased number of hydrogen bonds, ultimately exposing portions of the lower surface energy CCl_4 substrate. The structure of the first few layers of water on both hydrophilic and hydrophobic substrates is an area of great scientific interest and ongoing research.[49] For example, the first layer of water on hydrophilic Pt(111) has recently been shown to have a wetting structure consisting of a mosaic of 5, 6, and 7 member rings.[50–52] On nominally hydrophobic graphene[5] and Au(111)[53] substrates water forms a metastable wetting bilayer ice structure in which all of the molecules have four hydrogen bonds. Whether or not such a metastable bilayer structure forms on other hydrophobic substrates, such as CCl_4, will require additional research which is beyond the scope of this paper.

Conclusions

Two distinct desorption regimes of CCl_4 covered by an ASW overlayer have been determined through a combination of TPD and RAIRS. Dewetting occurs at various combinations of low H_2O coverage and high deposition temperatures resulting in a mixture of free and overlayer restricted CCl_4 desorption. The intensity of this low temperature CCl_4

desorption allows for the determination of the extent of dewetting by measuring the exposed CCl_4 surface area. Formation of a continuous ASW overlayer results in the rapid episodic release of CCl_4 in an event known as the ''molecular volcano''. Eruption of the volcano is directly correlated to the crystallization of the ASW overlayer and crystallization is dependent upon the ASW thickness and deposition temperature. Ongoing and future work in our laboratory focuses on determining the structure, kinetics, and energetics of nanoscale water films on CCl_4 and other hydrophobic surfaces.

Acknowledgements

This work was supported by the U.S. Department of Energy (DOE), Office of Basic Energy Sciences, Division of Chemical Sciences, Geosciences, and Biosciences. The research was performed using EMSL, a national scientific user facility sponsored by DOE's Office of Biological and Environmental Research and located at Pacific Northwest National Laboratory, which is operated by Battelle operated for the U.S. Department of Energy under Contract DE-AC05-76RL01830.

References

1 J. Israelachvili and H. Wennerstrom, *Nature*, 1996, **379**, 219–225.
2 N. T. Southall, K. A. Dill and A. D. J. Haymet, *J. Phys. Chem. B*, 2002, **106**, 521–533.
3 J. G. Huddleston, A. E. Visser, W. M. Reichert, H. D. Willauer, G. A. Broker and R. D. Rogers, *Green Chem.*, 2001, **3**, 156–164.
4 P. Ayotte, R. S. Smith, K. P. Stevenson, Z. Dohnalek, G. A. Kimmel and B. D. Kay, *J. Geophys. Res.*, 2001, **106**, 33387–33392.
5 G. A. Kimmel, J. Matthiesen, M. Baer, C. J. Mundy, N. G. Petrik, R. S. Smith, Z. Dohnalek and B. D. Kay, *J. Am. Chem. Soc.*, 2009, **131**, 12838–12844.
6 R. S. Smith, Z. Dohnalek, G. A. Kimmel, K. P. Stevenson and B. D. Kay, *Chem. Phys.*, 2000, **258**, 291–305.
7 R. J. Speedy, P. G. Debenedetti, R. S. Smith, C. Huang and B. D. Kay, *J. Chem. Phys.*, 1996, **105**, 240–244.
8 R. S. Smith, J. Matthiesen, J. Knox and B. D. Kay, *J. Phys. Chem. A*, 2011, **115**, 5908–5917.
9 P. Lofgren, P. Ahlstrom, J. Lausma, B. Kasemo and D. Chakarov, *Langmuir*, 2003, **19**, 265–274.
10 D. W. Flaherty, R. A. May, S. P. Berglund, K. J. Stevenson and C. B. Mullins, *Chem. Mater.*, 2010, **22**, 319–329.
11 R. A. May, D. W. Flaherty, C. B. Mullins and K. J. Stevenson, *J. Phys. Chem. Lett.*, 2010, **1**, 1264–1268.
12 K. P. Stevenson, G. A. Kimmel, Z. Dohnalek, R. S. Smith and B. D. Kay, *Science*, 1999, **283**, 1505–1507.
13 D. Schmidt, T. Hofmann, C. M. Herzinger, E. Schubert and M. Schubert, *Appl. Phys. Lett.*, 2010, **96**, 091906.
14 G. A. Kimmel, Z. Dohnalek, K. P. Stevenson, R. S. Smith and B. D. Kay, *J. Chem. Phys.*, 2001, **114**, 5295–5303.
15 G. A. Kimmel, K. P. Stevenson, Z. Dohnalek, R. S. Smith and B. D. Kay, *J. Chem. Phys.*, 2001, **114**, 5284–5294.
16 T. Zubkov, R. S. Smith, T. R. Engstrom and B. D. Kay, *J. Chem. Phys.*, 2007, **127**, 184707.
17 R. S. Smith, T. Zubkov, Z. Dohnalek and B. D. Kay, *J. Phys. Chem. B*, 2009, **113**, 4000–4007.
18 T. Zubkov, R. S. Smith, T. R. Engstrom and B. D. Kay, *J. Chem. Phys.*, 2007, **127**.
19 G. A. Kimmel, N. G. Petrik, Z. Dohnalek and B. D. Kay, *Phys. Rev. Lett.*, 2005, **95**, 166102.
20 G. A. Kimmel, N. G. Petrik, Z. Dohnalek and B. D. Kay, *J. Chem. Phys.*, 2006, **125**, 044713.
21 G. A. Kimmel, N. G. Petrik, Z. Dohnalek and B. D. Kay, *J. Chem. Phys.*, 2007, **126**, 114702.
22 D. Chandler, *Nature*, 2005, **437**, 640–647.
23 D. Chandler, *Nature*, 2007, **445**, 831–832.
24 T. W. Richards and E. K. Carver, *J. Am. Chem. Soc.*, 1921, **43**, 827–847.
25 J. C. Bonnet and F. P. Pike, *J. Chem. Eng. Data*, 1972, **17**, 145–150.
26 N. Giovambattista, P. G. Debenedetti and P. J. Rossky, *J. Phys. Chem. C*, 2007, **111**, 1323–1332.
27 N. Giovambattista, P. G. Debenedetti and P. J. Rossky, *Proc. Natl. Acad. Sci. U. S. A.*, 2009, **106**, 15181–15185.
28 N. Giovambattista, P. J. Rossky and P. G. Debenedetti, *J. Phys. Chem. B*, 2009, **113**, 13723–13734.
29 N. Giovambattista, P. J. Rossky and P. G. Debenedetti, *Phys. Rev. Lett.*, 2009, **102**, 050603.
30 M. Mezger, H. Reichert, S. Schoder, J. Okasinski, H. Schroder, H. Dosch, D. Palms, J. Ralston and V. Honkimaki, *Proc. Natl. Acad. Sci. U. S. A.*, 2006, **103**, 18401–18404.
31 A. Poynor, L. Hong, I. K. Robinson, S. Granick, Z. Zhang and P. A. Fenter, *Phys. Rev. Lett.*, 2006, **97**, 266101.
32 R. S. Smith, C. Huang, E. K. L. Wong and B. D. Kay, *Phys. Rev. Lett.*, 1997, **79**, 909–912.
33 R. S. Smith, T. Zubkov and B. D. Kay, *J. Chem. Phys.*, 2006, **124**, 114710.
34 S. L. Tait, Z. Dohnalek, C. T. Campbell and B. D. Kay, *J. Chem. Phys.*, 2006, **125**, 234308.
35 R. S. Smith, N. G. Petrik, G. A. Kimmel and B. D. Kay, *Acc. Chem. Res.*, 2011, DOI: 10.1021/ar200070w.
36 V. Sadtchenko, K. Knutsen, C. F. Giese and W. R. Gentry, *J. Phys. Chem. B*, 2000, **104**, 4894–4902.
37 V. Sadtchenko, K. Knutsen, C. F. Giese and W. R. Gentry, *J. Phys. Chem. B*, 2000, **104**, 2511–2521.
38 Z. Dohnalek, G. A. Kimmel, R. L. Ciolli, K. P. Stevenson, R. S. Smith and B. D. Kay, *J. Chem. Phys.*, 2000, **112**, 5932–5941.
39 P. Lofgren, P. Ahlstrom, D. V. Chakarov, J. Lausmaa and B. Kasemo, *Surf. Sci.*, 1996, **367**, L19–L25.
40 G. Zimbitas, S. Haq and A. Hodgson, *J. Chem. Phys.*, 2005, **123**, 174701.
41 D. J. Safarik, R. J. Meyer and C. B. Mullins, *J. Chem. Phys.*, 2003, **118**, 4660–4671.
42 D. J. Safarik and C. B. Mullins, *J. Chem. Phys.*, 2004, **121**, 6003–6010.
43 T. R. Linderoth, V. P. Zhdanov and B. Kasemo, *Phys. Rev. Lett.*, 2003, **90**, 156103.
44 J. P. Devlin, *J. Geophys. Res.*, 2001, **106**, 33333–33349.
45 J. Matthiesen, R. S. Smith and B. D. Kay, *Phys. Rev. Lett.*, 2009, **103**, 245902.
46 R. S. Smith, J. Matthiesen and B. D. Kay, *J. Chem. Phys.*, 2010, **132**, 124502.
47 R. S. Smith, J. Matthiesen and B. D. Kay, *J. Chem. Phys.*, 2010, **133**, 174504.
48 J. Matthiesen, R. S. Smith and B. D. Kay, *J. Chem. Phys.*, 2010, **133**, 174505.
49 A. Hodgson and S. Haq, *Surf. Sci. Rep.*, 2009, **64**, 381–451.
50 P. J. Feibelman, N. C. Bartelt, S. Nie and K. Thurmer, *J. Chem. Phys.*, 2010, **133**, 154703.
51 S. Nie, P. J. Feibelman, N. C. Bartelt and K. Thurmer, *Phys. Rev. Lett.*, 2010, **105**, 026102.
52 P. J. Feibelman, G. A. Kimmel, R. S. Smith, N. G. Petrik, T. Zubkov and B. D. Kay, *J. Chem. Phys.*, 2011, **134**, 204702.
53 D. Stacchiola, J. B. Park, P. Liu, S. Ma, F. Yang, D. E. Starr, E. Muller, P. Sutter and J. Hrbek, *J. Phys. Chem. C*, 2009, **113**, 15102–15105.